

Behaviour of the Serre Equations for the Dam-Break Problem

Jordan Pitt,¹
Christopher Zoppou,¹
Stephen G. Roberts,¹

ABSTRACT

Keywords: dispersive waves, conservation laws, Serre equation, finite volume method, finite difference method

1 INTRODUCTION

2 The dam break problem is a classical problem in shallow water modelling. Its
3 main challenge is that it contains a discontinuity in the initial conditions at the dam
4 wall. For some equations such as the Shallow Water Wave equations (SWWE) this
5 is not a problem for finite volume based numerical methods (Zoppou and Roberts
6 2003) as they're in conservative form. For dispersive shallow water models such as
7 the Serre equations this discontinuity does present an issue as the equations usually
8 require certain smoothness of the initial conditions and aren't in conservative form
9 (Mitsotakis et al. 2014).

10 The dam break problem for a dispersive model results in undular bores as the sharp
11 shock front decomposes into solitary waves at the shock front (Peregrine 1966). Cor-
12 rectly modelling dispersion is important to accurately represent a range of fluid prob-
13 lems from tidal bores to tsunamis (Glimsdal et al. 2013). Shoaling of waves can also
14 result in very steep gradients and so to have accurate models of the nearshore behaviour
15 of fluids requires methods that are robust to large gradients in water depth.

16 Our equations of interest are the Serre equations (Serre 1953; Su and Gardner 1969;
17 Seabra-Santos et al. 1981; Green and Naghdi 1976), which up to wave breaking are
18 considered a very good approximation to the full water wave problem in shallow water
19 (Bonneton et al. 2011). The literature around numerical methods for the Serre equa-
20 tions deal with the problem in many ways from simple finite difference methods (FDM)
21 (Antunes do Carmo et al. 1993; Nwogu 1993; El et al. 2006) to finite element methods
22 (FEM) (Li et al. 2014; Mitsotakis et al. 2014) and even hybrid finite difference-volume

¹Mathematical Sciences Institute, Australian National University, Canberra, ACT 0200, Australia,
E-mail: Jordan.Pitt@anu.edu.au. The work undertaken by the first author was supported financially by
an Australian National University Scholarship.

hybrid methods (FDVHM) (Le Métayer et al. 2010; Zoppou et al. 2017; Filippini et al. 2016; Bradford and Sanders 2002). There are however little results concerning discontinuities or even very steep gradients (El et al. 2006; Le Métayer et al. 2010; Mitsotakis et al. 2014). Among these results only one handles the problem well (El et al. 2006) with the others only presenting very shallow analysis of the problem (Le Métayer et al. 2010; Mitsotakis et al. 2014). There is also disagreement among these papers about the nature of these solutions.

The aim of this paper is then to further investigate the dam break problem and the behaviour of steep gradients for the Serre equations. To do this we make use of a first, second and third order numerical method that is robust to steep gradients, with the first order method being a recreation of the numerical method of Le Métayer et al. (2010). For comparison we use two finite difference schemes, one being the naive one and the other being a recreation of the method of El et al. (2006). Since some papers (Mitsotakis et al. 2014; El et al. 2006) have used smoothing of the initial conditions to handle discontinuities we do the same and investigate the effects of various steepness on the results of our numerical methods as well. We also present analytic comparisons that have been used in the literature the SWWE analytic results for the dam break problem (Wu et al. 1999) and Whitham modulation results by El et al. (2006).

The paper is organised as follows: The Serre equations are given as well as some important properties for validation, a reproducible explanation of the two FD methods are given as well as the reformulation of the Serre equations into conservative form, then some numerical results are given for the soliton problem to validate the FD methods and then our investigation into the behaviour of the Serre equations applied to the dam break problem.

SERRE EQUATIONS

The Serre equations can be derived by integrating the full incompressible Euler equations over the water depth, see for example Su and Gardner (1969). They can also be derived as an asymptotic expansion of the Euler equations, see for example Lannes and Bonneton (2009). Assuming a constant horizontal bed the Serre equations are (Li et al. 2014)

$$\frac{\partial h}{\partial t} + \frac{\partial(uh)}{\partial x} = 0 \quad (1a)$$

$$\underbrace{\frac{\partial(uh)}{\partial t} + \frac{\partial}{\partial x} \left(u^2 h + \frac{gh^2}{2} \right)}_{\text{Shallow Water Wave Equations}} + \underbrace{\frac{\partial}{\partial x} \left(\frac{h^3}{3} \left[\frac{\partial u}{\partial x} \frac{\partial u}{\partial x} - u \frac{\partial^2 u}{\partial x^2} - \frac{\partial^2 u}{\partial x \partial t} \right] \right)}_{\text{Dispersion Terms}} = 0. \quad (1b)$$

Serre Equations

Where u is the average horizontal velocity over the depth of water h and g is the acceleration due to gravity.

Conservation Laws

The Serre equations conserve a number of physical quantities, thus our numerical methods should reflect this. The total of a quantity q in a system is measured by

$$\mathcal{C}_q(t) = \int_{-\infty}^{\infty} q \, dx \quad (2)$$

so that we have for all t both $\mathcal{C}_h(0) = \mathcal{C}_h(t)$, $\mathcal{C}_{uh}(0) = \mathcal{C}_{uh}(t)$ and $\mathcal{C}_{\mathcal{H}}(0) = \mathcal{C}_{\mathcal{H}}(t)$ which represents conservation of mass, momentum and the Hamiltonian (Li 2002; Le Métayer et al. 2010; Green and Naghdi 1976) respectively. The Hamiltonian is

$$\mathcal{H}(x, t) = \frac{1}{2} \left(hu^2 + \frac{h^3}{3} \left(\frac{\partial u}{\partial x} \right)^2 + gh^2 \right). \quad (3)$$

it represents the energy in the system and is the sum of the kinetic energies in the horizontal and vertical directions and the gravitational potential energy respectively.

DIRECT NUMERICAL METHODS FOR SOLVING THE SERRE EQUATIONS

The presence of the mixed spatial temporal derivatives in the momentum equation (1b) makes the Serre equations difficult to solve with standard numerical methods. A naive way to avoid this is to approximate (1b) by finite differences and the results of this are presented here.

Finite Difference Approximation to Conservation of Momentum Equation

Zoppou et al. (2017) demonstrated that a numerical scheme for solving the Serre equations must be at least second-order accurate. Therefore, the derivatives in (1b) will be approximated by second-order finite differences. Firstly (1b) must be expanded, making use of (1a) one obtains

$$h \frac{\partial u}{\partial t} + X - h^2 \frac{\partial^2 u}{\partial x \partial t} - \frac{h^3}{3} \frac{\partial^3 u}{\partial x^2 \partial t} = 0 \quad (4a)$$

where X contains only spatial derivatives and is

$$X = uh \frac{\partial u}{\partial x} + gh \frac{\partial h}{\partial x} + h^2 \frac{\partial u}{\partial x} \frac{\partial u}{\partial x} + \frac{h^3}{3} \frac{\partial u}{\partial x} \frac{\partial^2 u}{\partial x^2} - h^2 u \frac{\partial^2 u}{\partial x^2} - \frac{h^3}{3} u \frac{\partial^3 u}{\partial x^3}. \quad (4b)$$

Taking the second-order centred finite difference approximation to the spatial and temporal derivatives for (4a) on a uniform grid in space and time with $\Delta x = x_{i+1} - x_i$ and $\Delta t = t^{n+1} - t^n$ for all i where $h_i = h(x_i)$ and $h^n = h(t^n)$ gives

$$h_i^n u_i^{n+1} - (h_i^n)^2 \left(\frac{u_{i+1}^{n+1} - u_{i-1}^{n+1}}{2\Delta x} \right) - \frac{(h_i^n)^3}{3} \left(\frac{u_{i+1}^{n+1} - 2u_i^{n+1} + u_{i-1}^{n+1}}{\Delta x^2} \right) = -Y_i^n \quad (5)$$

where

$$Y_i^n = 2\Delta t X_i^n - h_i^n u_i^{n-1} + (h_i^n)^2 \left(\frac{u_{i+1}^{n-1} - u_{i-1}^{n-1}}{2\Delta x} \right) + \frac{(h_i^n)^3}{3} \left(\frac{u_{i+1}^{n-1} - 2u_i^{n-1} + u_{i-1}^{n-1}}{\Delta x^2} \right)$$

Equation (5) can be rearranged into an explicit update scheme for u given its current and previous values, so that

$$\begin{bmatrix} u_0^{n+1} \\ \vdots \\ u_m^{n+1} \end{bmatrix} = A^{-1} \begin{bmatrix} -Y_0^n \\ \vdots \\ -Y_m^n \end{bmatrix} =: \mathcal{G}_u(\mathbf{u}^n, \mathbf{h}^n, \mathbf{u}^{n-1}, \Delta x, \Delta t) \quad (6)$$

where A is a tri-diagonal matrix.

The Lax Wendroff Method for Conservation of Mass Equation

The conservation of mass equation (1a) has no mixed derivative term standard numerical techniques for conservation laws can be used. In particular the Lax-Wendroff method as done by El et al. (2006), here we present the method in replicable detail.

Note that (1a) is in conservative law form for h where the flux is uh . Thus using the previously defined spatio-temporal discretisation the two step Lax-Wendroff update for h is

$$h_{i+1/2}^{n+1/2} = \frac{1}{2} (h_{i+1}^n + h_i^n) - \frac{\Delta t}{2\Delta x} (u_{i+1}^n h_{i+1}^n - h_i^n u_i^n), \quad (7)$$

$$h_{i-1/2}^{n+1/2} = \frac{1}{2} (h_i^n + h_{i-1}^n) - \frac{\Delta t}{2\Delta x} (u_i^n h_i^n - h_{i-1}^n u_{i-1}^n) \quad (8)$$

and

$$h_i^{n+1} = h_i^n - \frac{\Delta t}{\Delta x} (u_{i+1/2}^{n+1/2} h_{i+1/2}^{n+1/2} - u_{i-1/2}^{n+1/2} h_{i-1/2}^{n+1/2}). \quad (9)$$

The quantities $u_{i\pm 1/2}^{n+1/2}$ are calculated using u^{n+1} obtained by applying \mathcal{G}_u to u^n then linear interpolation in both space and time gives

$$u_{i+1/2}^{n+1/2} = \frac{u_{i+1}^{n+1} + u_{i+1}^n + u_i^{n+1} + u_i^n}{4} \quad (10)$$

and

$$u_{i-1/2}^{n+1/2} = \frac{u_i^n + u_i^n + u_{i-1}^{n+1} + u_{i-1}^n}{4}. \quad (11)$$

Thus we have the following update scheme for (1a)

$$\mathbf{h}^{n+1} = \mathcal{E}_h(\mathbf{u}^n, \mathbf{h}^n, \mathbf{u}^{n+1}, \Delta x, \Delta t). \quad (12)$$

The update scheme for all of (1) is

$$\left. \begin{aligned} \mathbf{u}^{n+1} &= \mathcal{G}_u(\mathbf{u}^n, \mathbf{h}^n, \mathbf{u}^{n-1}, \Delta x, \Delta t) \\ \mathbf{h}^{n+1} &= \mathcal{E}_h(\mathbf{u}^n, \mathbf{h}^n, \mathbf{u}^{n+1}, \Delta x, \Delta t) \end{aligned} \right\} \mathcal{E}(\mathbf{u}^n, \mathbf{h}^n, \mathbf{u}^{n-1}, \mathbf{h}^{n-1}, \Delta x, \Delta t). \quad (13)$$

114 Second-Order Naive Finite Difference Method

115 Here we also present a completely naive method for comparative purposes, to do
 116 this we apply the procedure used above on (1b) and (1a). The derivatives are expanded
 117 then approximated by second-order centered finite differences after rearranging this to
 118 give an update formula we obtain

$$119 \quad h_i^{n+1} = h_i^{n-1} - \Delta t \left(u_i^n \frac{h_{i+1}^n - h_{i-1}^n}{\Delta x} + h_i^n \frac{u_{i+1}^n - u_{i-1}^n}{\Delta x} \right). \quad (14)$$

121 Performing this update for all i will be denoted by $\mathcal{G}_h(\mathbf{u}^n, \mathbf{h}^n, \mathbf{h}^{n-1}, \Delta x, \Delta t)$. Thus
 122 we get the naive second-order centred finite difference method for the Serre equations

$$123 \quad \left. \begin{aligned} \mathbf{h}^{n+1} &= \mathcal{G}_h(\mathbf{u}^n, \mathbf{h}^n, \mathbf{h}^{n-1}, \Delta x, \Delta t) \\ \mathbf{u}^{n+1} &= \mathcal{G}_u(\mathbf{u}^n, \mathbf{h}^n, \mathbf{u}^{n-1}, \Delta x, \Delta t) \end{aligned} \right\} \mathcal{G}(\mathbf{u}^n, \mathbf{h}^n, \mathbf{u}^{n-1}, \mathbf{h}^{n-1}, \Delta x, \Delta t). \quad (15)$$

126 CONSERVATIVE FORM OF THE SERRE EQUATIONS

127 To overcome the aforementioned difficulty of mixed derivatives the Serre equations
 128 (1) can be reformulated into conservative form. This is accomplished by the introduc-
 129 tion of a new quantity (Le Métayer et al. 2010; Zoppou 2014)

$$130 \quad G = uh - h^2 \frac{\partial h}{\partial x} \frac{\partial u}{\partial x} - \frac{h^3}{3} \frac{\partial^2 u}{\partial x^2}. \quad (16)$$

132 Consequently, (1) can be rewritten as

$$133 \quad \frac{\partial h}{\partial t} + \frac{\partial(uh)}{\partial x} = 0 \quad (17a)$$

135 and

$$136 \quad \frac{\partial G}{\partial t} + \frac{\partial}{\partial x} \left(Gu + \frac{gh^2}{2} - \frac{2h^3}{3} \frac{\partial u}{\partial x} \frac{\partial u}{\partial x} \right) = 0. \quad (17b)$$

139 A Hybrid Finite Difference-Volume Method for Serre Equations in Conservative Form

140 The conservative form (17) allows for a wider range of numerical techniques such
 141 as finite element methods (Li et al. 2014) and finite volume methods (Le Métayer et al.
 142 2010; Zoppou 2014). In this paper the first (\mathcal{V}_1), second (\mathcal{V}_2) and third-order (\mathcal{V}_3) finite
 143 difference-volume methods (FDVM) of Zoppou et al. (2017) will be used. These have
 144 been validated and their order of accuracy confirmed.
 145

Stability Condition

To ensure stability of the FDVMs the time-step Δt must satisfy the Courant-Friedrichs-Lewy (CFL) criteria (A. Harten 1983)

$$\Delta t < \frac{Cr\Delta x}{2 \max\{|\lambda|\}} \quad (18)$$

with $0 < Cr \leq 1$ where λ is the characteristic speed. For the Serre equations it has been demonstrated that the wave speed is bounded by the characteristic speed of the Shallow Water Wave equations (Le Métayer et al. 2010). [stability for the two FD methods]

NUMERICAL SIMULATIONS

In this section the methods introduced in this paper will be validated by using them to approximate an analytic solution of the Serre equations, this will also be used to verify their order of accuracy. Then an in-depth comparison of these methods for a smooth approximation to the discontinuous dam break problem will be provided to investigate the behaviour of these numerical schemes in the presence of steep gradients. This is a problem that so far has only received a proper treatment in (El et al. 2006), with other research giving only a cursory investigation into the topic. [][refs]

SOLITON

Currently cnoidal waves are the only family of analytic solutions to the Serre equations (Carter and Cienfuegos 2011). Solitons are a particular instance of cnoidal waves that travel without deformation which has been used to verify the convergence rates of the described methods in this paper.

For the Serre equations the solitons have the following form

$$h(x, t) = a_0 + a_1 \text{sech}^2(\kappa(x - ct)), \quad (19a)$$

$$u(x, t) = c \left(1 - \frac{a_0}{h(x, t)} \right), \quad (19b)$$

$$\kappa = \frac{\sqrt{3a_1}}{2a_0\sqrt{a_0 + a_1}} \quad (19c)$$

and

$$c = \sqrt{g(a_0 + a_1)} \quad (19d)$$

where a_0 and a_1 determine the depth of the quiescent water and the maximum height of the soliton above that respectively. In the simulation $a_0 = 1\text{m}$, $a_1 = 0.7\text{m}$ for $x \in [-50\text{m}, 250\text{m}]$ and $t \in [0\text{s}, 50\text{s}]$. With $\Delta t = 0.5\lambda^{-1}\Delta x$ where $\lambda = \sqrt{g(a_0 + a_1)}$ which is the maximum wave speed, this satisfies the CFL condition (18).

Results

This numerical experiment and its results for the FDVM have been reported by Zoppou et al. (2017), this paper only reports the results for \mathcal{G} and \mathcal{E} . From Figure 1(a) it can be seen that \mathcal{G} and \mathcal{E} accurately model the highly non-linear soliton problem reproducing the analytic solution up to graphical accuracy.

To demonstrate that in fact \mathcal{E} and \mathcal{G} are consistent, two measures were used. The first measures the relative distance of the numerical results for h and u from the analytic solution, it is defined for a general quantity q and an approximation to it q^* at n values

$$L_1 = \frac{\sum_{i=1}^n |q_i - q_i^*|}{\sum_{i=1}^n |q_i|}. \quad (20)$$

The second measures how well the schemes conserve a quantity q over time

$$C_1 = \frac{|\mathcal{C}_q(0) - \mathcal{C}_{q^*}(t_f)|}{|\mathcal{C}_q(0)|} \quad (21)$$

where t_f is the final time of the numerical experiment. For $\mathcal{C}_q(0)$ the analytic value is used while a numerical calculation is used for $\mathcal{C}_{q^*}(t_f)$ based on summing cell-wise integrals. For h and uh for all our schemes either have the cell-wise average or the midpoint is equivalent to it up to sufficient order so multiplying the cell-wise averages by Δx gives the cell-wise integral for h and uh . The cell-wise integral for \mathcal{H} is calculated by quartic interpolation of h and u utilizing neighboring cells and then applying Gaussian quadrature with 3 points over the cell to get a sufficiently high order approximation, in particular it is at least third-order accurate for the $\partial u / \partial x$ term. From Figure 2 it can be seen that both FD methods are convergent under L_1 with second-order accuracy. There is however suboptimal rates of convergence for very small Δx due to round off effects and large Δx due to the initial conditions not being accurately represented on a coarse grid.

Figure 2 demonstrates conservation of both mass and momentum to at least second-order for both FD schemes. Both schemes conserve mass very well with round off error dominance occurring at the same place as for L_1 . Momentum has the appropriate order of accuracy for larger Δx but then stagnates as Δx decreases. This is due to the use of a finite difference method which is not necessarily conservative. Surprisingly the Hamiltonian is conserved with an order of accuracy greater than the momentum, with the effects of round off errors occurring earlier due to the greater number of calculations.

All of these measures demonstrate that \mathcal{G} and \mathcal{E} are appropriate to solve highly non-linear problems with smooth initial conditions for the Serre equations.

SMOOTHED DAM-BREAK

The discontinuous dam-break problem can be approximated smoothly using the hyperbolic tangent function. Such an approximation will be called a smoothed dam-break problem and will be defined as such

$$h(x, 0) = h_0 + \frac{h_1 - h_0}{2} \left(1 + \tanh \left(\frac{x_0 - x}{\alpha} \right) \right), \quad (22a)$$

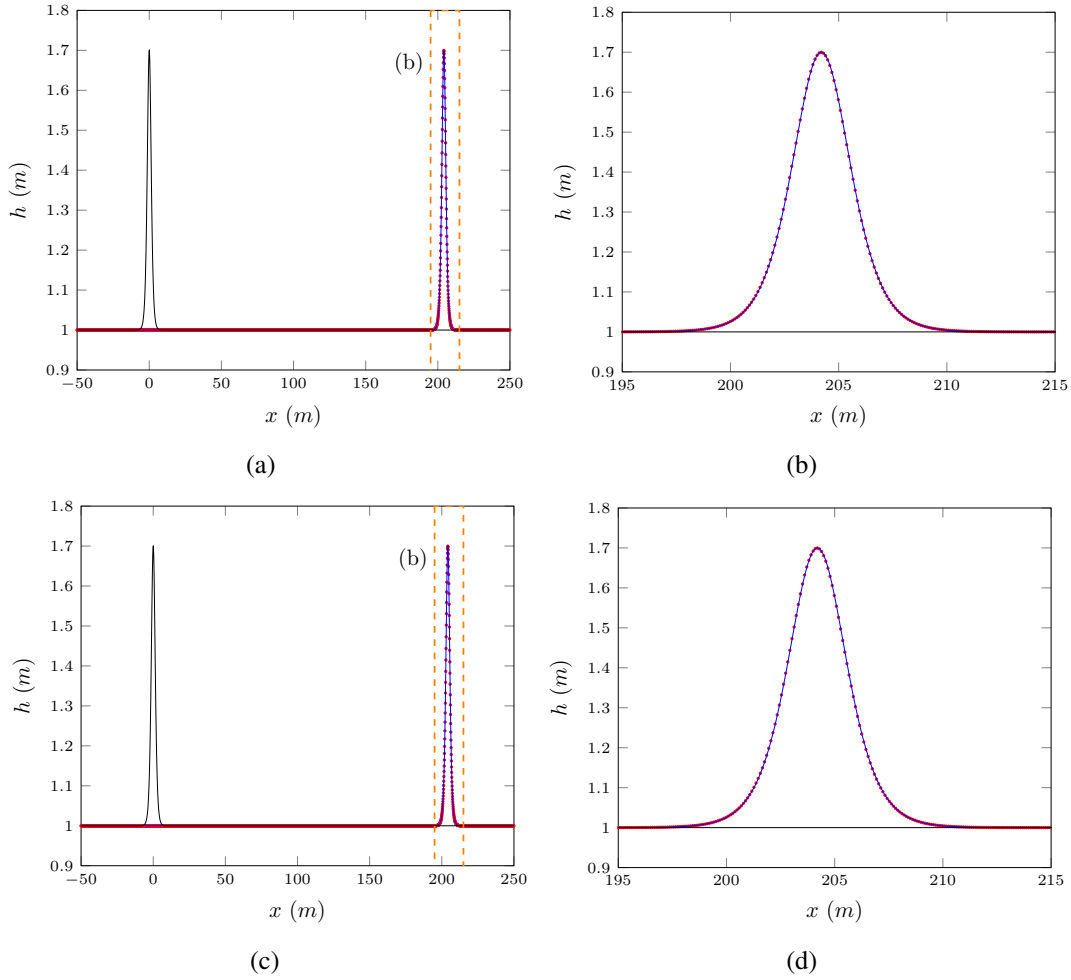


FIG. 1: Water profile for the soliton problem (6) for \mathcal{G} ((a),(b)) and \mathcal{E} ((c),(d)) when $\Delta x = 10/2^{12}$ with the initial conditions (—), analytic solution (—) and numerical result (•).

214

215
216

$$u(x, 0) = 0.0 \text{ m/s.} \quad (22b)$$

217 Where α is given and controls the width of the transition between the two dam-break
 218 heights of h_0 and h_1 . α measures the distance over which 46.117% of the transition
 219 between h_0 and h_1 centered around x_0 occurs. Figure 3 demonstrates various smoothed
 220 dam break problems with different α values.

221 The dam break problem for the Serre equations results in the creation of an undular
 222 bore that is very similar to the analytic solution of the dam break problem for the
 223 SWWE with oscillations occurring on top (Le Métayer et al. 2010). Because of this
 224 some values from the analytic solution to the dam break problem for the SWWE will
 225 be used as a reference in this paper; these are the height (h_2) and velocity (u_2) in the
 226 shock as well as the speed of the shock front (S_2). From Wu et al. (1999) we have the

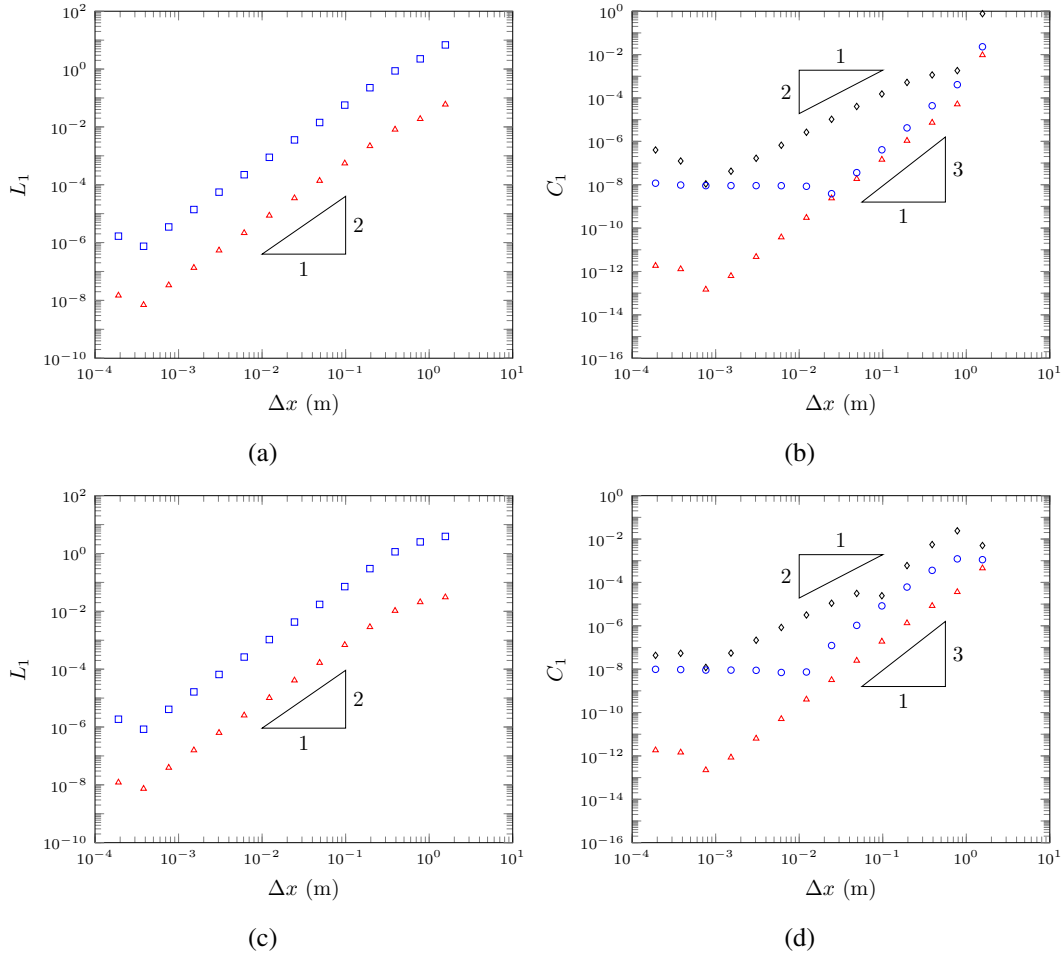


FIG. 2: On the left L_1 errors for h (\triangle) and u (\square) and on the right H_1 (\circ) for the soliton problem with (a) and (b) for \mathcal{G} and (c) and (d) for \mathcal{E} .

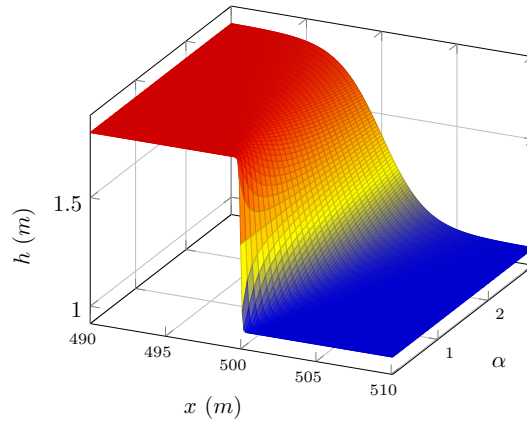


FIG. 3: Initial conditions for the smooth dambreak problem for various α .

227 following equations

$$228 \quad h_2 = \frac{h_0}{2} \left[\sqrt{1 + 8 \left(\frac{2h_2}{h_2 - h_0} \frac{\sqrt{gh_1} - \sqrt{gh_2}}{\sqrt{gh_0}} \right)^2} - 1 \right], \quad (23)$$

229
230

$$231 \quad u_2 = 2 \left(\sqrt{gh_1} - \sqrt{gh_2} \right) \quad (24)$$

232

233 and

$$234 \quad S_2 = \frac{h_2 u_2}{h_2 - h_0}. \quad (25)$$

235

236 Undular bores for the one dimensional Serre equations were analysed by El et al.
237 (2006) and an expression for the amplitude (a^+) and speed (S^+) of the leading wave
238 of a bore was given

$$239 \quad \frac{\Delta}{(a^+ + 1)^{1/4}} - \left(\frac{3}{4 - \sqrt{a^+ + 1}} \right)^{21/10} \left(\frac{2}{1 + \sqrt{a^+ + 1}} \right)^{2/5} = 0 \quad (26)$$

240

241 and

$$242 \quad S^+ = \sqrt{g(a^+ + 1)} \quad (27)$$

243

244 where $\Delta = h_r/h_0$, and h_r is the amplitude of the bore.

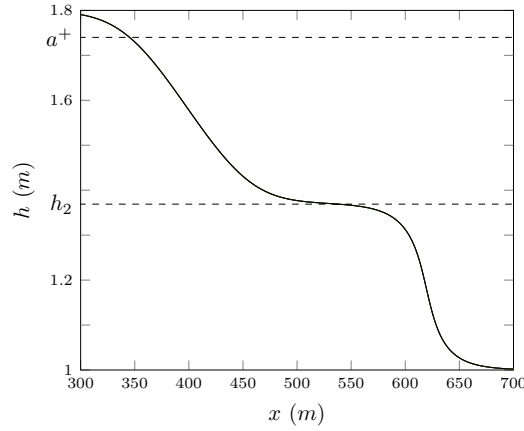
In these experiments $h_0 = 1.0m$, $h_1 = 1.8m$ and $x_0 = 500m$. This scenario replicates one presented by El et al. (2006) and Le Métayer et al. (2010). The simulations were run with various values of Δx and β . To ensure stability especially of the FD methods a very restrictive time step of $\Delta t = 0.01\Delta x$ was chosen and for $\mathcal{V}_2 \theta = 1.2$. From this description the Hamiltonian at the initial time is

$$\mathcal{H}(0) = 10398.6 - 0.7848 \times \left[\frac{2}{\alpha} \tanh(500\alpha) \right]. \quad (28)$$

245 Applying (23), (24) and (25) to these initial conditions results in $h_2 = 1.36898m$,
246 $u_2 = 1.074975 m/s$ and $S_2 = 3.98835 m/s$. For (26) and (27) the process is a little
247 different because $h_r \neq h_2$ but instead comes from the intersection of the Riemann
248 invariant curve and the centred left propagating rarefaction wave curve (El et al. 2006),
249 which results in $h_r = 1.37082$ thus $\Delta = 1.37082$, $a^+ = 1.73998 m$ and $S^+ = 4.13148$
250 m/s . Of particular note is that due to the different natures of bores for the Serre and
251 SWE equations $S^+ \neq S_2$.

252 Results

253 We begin this study by looking into the effect of the initial steepness of the smoothed
254 dam break problem for different β values observing what happens as $\Delta x \rightarrow 0$ and our
255 numerical solution better approximates the true solution of the Serre equations. To this
256 end we use the highest order well validated model \mathcal{V}_3 in the following investigation.
257 From these results we then investigate numerical results for long time scales, how the
258 SWE analytic values and Elswham modulation values compare to our results and
259 then finally present some other findings about the behaviour of our numerical solutions.



(a)

FIG. 4: Numerical results of \mathcal{V}_3 at $t = 30s$ for the smooth dam break problem with $\beta = 117.778$ for $\Delta x = 10/2^{10}$ (—), $\Delta x = 10/2^9$ (—), $\Delta x = 10/2^8$ (—), $\Delta x = 10/2^7$ (—), $\Delta x = 10/2^6$ (—), $\Delta x = 10/2^5$ (—), $\Delta x = 10/2^4$ (—) with reference value a^+ (—).

effect of β

Because the smoothing process is a non physical numerical tool we will first study its effect by decreasing β and thus better approximating the dam break. To do this we fix a β and then investigate the numerical solutions as $\Delta x \rightarrow 0$ and our well validated numerical methods better approximate the true solution of the equations.

The first and most important observation is that there are four types of behaviour as $\Delta x \rightarrow 0$ depending on the β and the numerical method. The four scenarios are identified by the behaviour of the solutions when Δx is small and they correspond to different results in the literature. For brevity the only given examples of these scenarios will be the solutions of \mathcal{V}_3 although they also occurred for \mathcal{E} , \mathcal{G} and \mathcal{V}_2 .

The first behaviour which will be referred to as the non-oscillatory scenario has such smooth initial conditions that no oscillations were introduced by $t = 30s$, although given sufficient time the front steepens and an undular bore develops. An example of this behaviour can be seen in Figure 4 for $\beta = 117.778$. Because this is a very smooth problem we observe rapid convergence with all the numerical results being graphically identical. This scenario resembles very diffusive solutions of the SWWE in that it contains only a rarefaction and a shock with no dispersive waves.

Convergence is also present in Figure 5 with both the L_1 and H_1 measures. However, L_1 has been modified to use the solution of the smallest Δx as an approximation to the analytic solution because none are currently known. For both measures the order of accuracy is the theoretical one, with round-off errors becoming dominant for small Δx . Since L_1 now compares only numerical results, round-off errors result in error stagnation rather than increase. For H_1 it can be seen that round-off errors are dominant earlier than in L_1 this is because H_1 requires many more calculations. This suggests that this family of solutions is also a true representation of the behaviour of the Serre equations when β is sufficiently large and in particular $\beta = 117.778$.

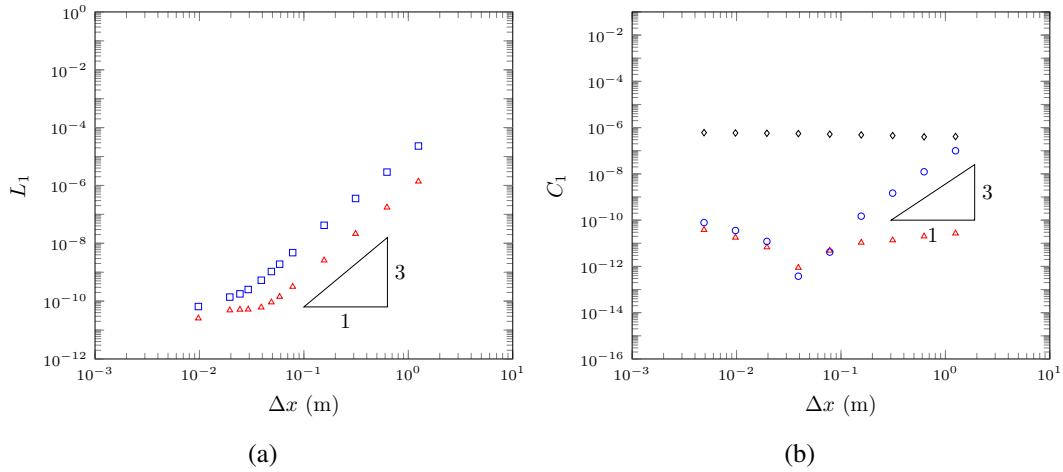


FIG. 5: L_1 for h (\triangle) and u (\square) and H_1 (\circ) for \mathcal{V}_3 's solution for the smooth dambreak problem with $\beta = 117.778$.

The second scenario will be referred to as the flat scenario due to the presence of a constant height state between the oscillations at the shock and rarefaction fan. An example of the numerical results for this scenario can be seen in Figure 6 when $\beta = 5.8889$. This scenario corresponds to the results presented by Le Métayer et al. (2010) and Mitsotakis et al. (2016).

As Δx decreases the solutions converge so that by $\Delta x = 10/2^8$ the solutions for higher Δx are visually identical. There is also good agreement between the amplitude of the leading soliton and a^+ as well as the plateau height and h_2 . Although as Δx is decreased the plateau seems to be slightly above this value. Since this method is well validated for smooth problems and a small Δx has been chosen this suggests that the bore from a dam break problem may differ slightly for the Serre and SWWE although they are still quite close. These results also compare well to the results in Mitsotakis et al. (2016) who use the same β but different h_0 and h_1 .

The measures L_1 and H_1 also demonstrate good convergence with the expected order of accuracy in the middle of the plot. Suboptimal convergence is expected for large Δx as the problem is not sufficiently resolved to model the oscillations and so both H_1 and L_1 suffer. For small Δx the measure H_1 becomes suboptimal due to round-off errors however this effect is masked by L_1 as a numerical solution is the base of the comparison instead of an analytic result.

The third scenario will be referred to as the contact discontinuity (El et al. 2006) scenario. The contact discontinuity scenarios main feature is that the oscillations from the rarefaction fan and the shock decay and appear to meet at a point as can be seen in Figure 8 when $\beta = 1.1778$. All the higher order methods so far have not shown a converged solution as Δx decreases. However, it does appear that convergence is likely with the solutions getting closer together, especially since for the smaller Δx this problem is still smooth. These results also compare very well in terms of the lead soliton amplitude and the bore height reference values given on the plots. This scenario

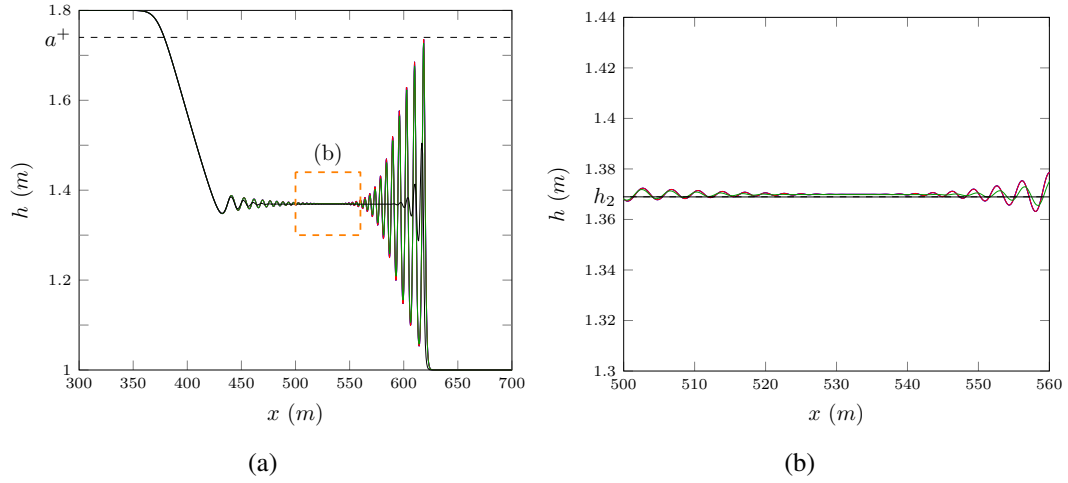


FIG. 6: Numerical results of \mathcal{V}_3 at $t = 30s$ for the smooth dam break problem with $\beta = 5.8888$ for $\Delta x = 10/2^{10}$ (—), $\Delta x = 10/2^9$ (—), $\Delta x = 10/2^8$ (—), $\Delta x = 10/2^7$ (—), $\Delta x = 10/2^6$ (—), $\Delta x = 10/2^5$ (—), $\Delta x = 10/2^4$ (—) with reference value a^+ (—).

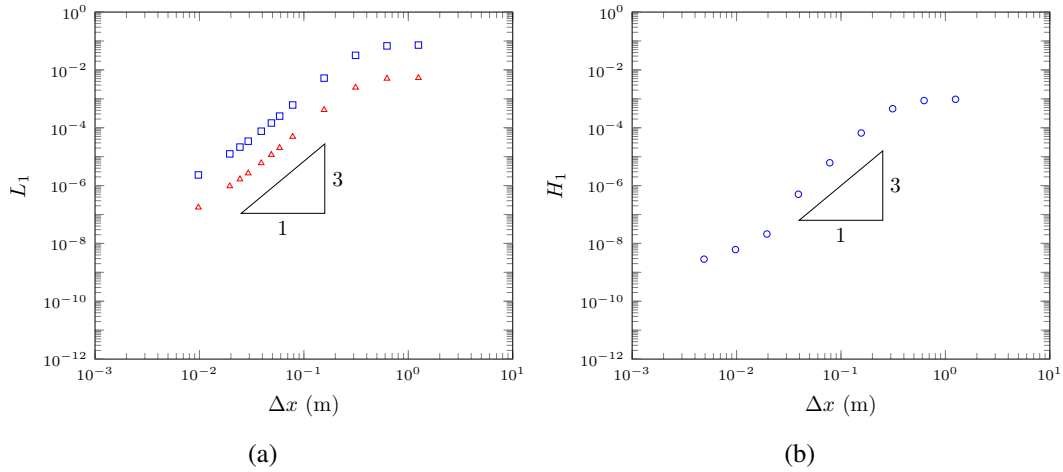


FIG. 7: L_1 for h (Δ) and u (\square) and H_1 (\circ) for \mathcal{V}_3 's solution for the smooth dambreak problem with $\beta = 5.8888$.

313 was observed by El et al. (2006) for \mathcal{E} and indeed we have replicated them for all the
 314 high order methods in this paper. The necessity of a β lower than 5.8889 to recover
 315 the ‘contact discontinuity’ explains why (Mitsotakis et al. 2016) could not replicate the
 316 results of (El et al. 2006).

317 The assertion that these results are close to converged is supported by Figure 9 for
 318 the L_1^* and H_1 measured. As can be seen in Figure 8(c) the final solutions have not yet
 319 even graphically converged, thus we modify L_1 to omit this section from $[520m, 540m]$
 320 and call this modified measure L_1^* . Thus L_1^* demonstrates that even though this middle
 321 section has not been fully resolved we do see that there is convergence at the appropri-
 322 ate order outside this region. Suggesting that the effect of better resolving this contact

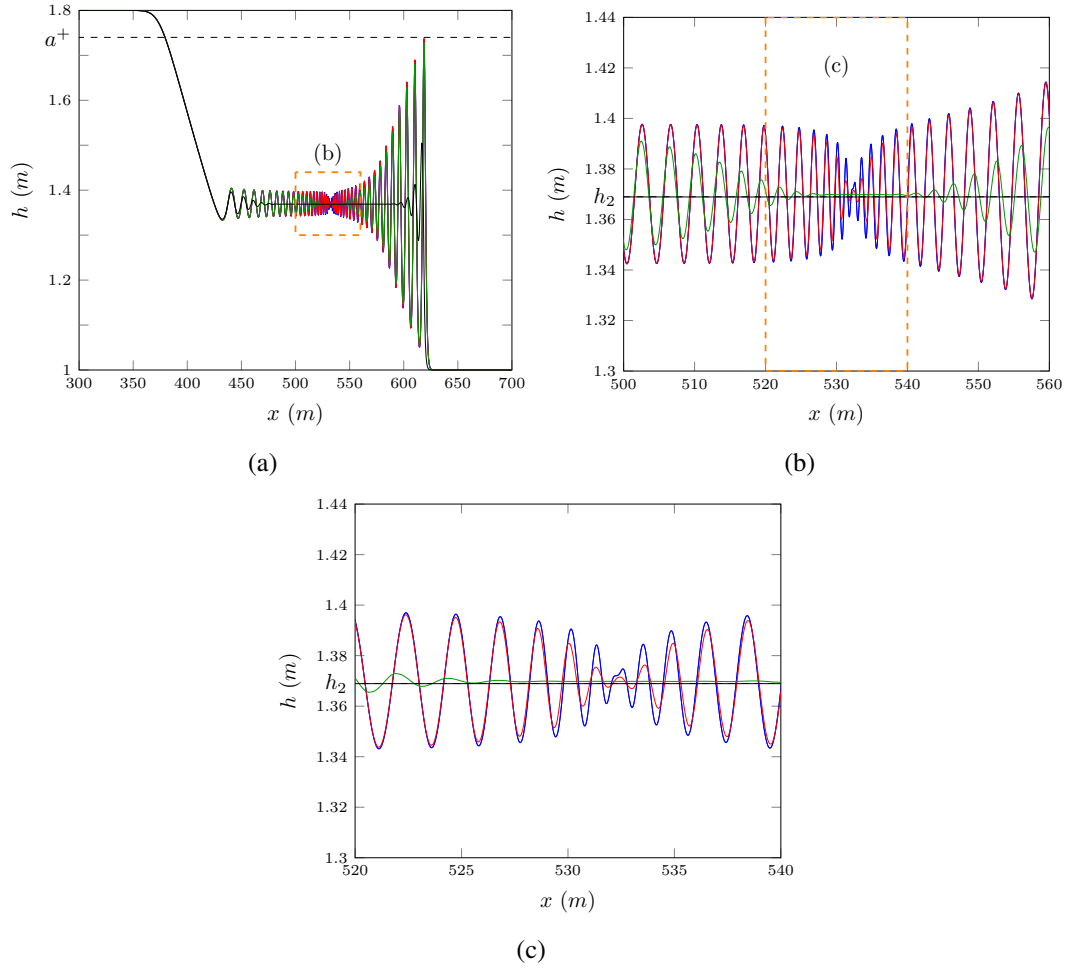


FIG. 8: Numerical results of \mathcal{V}_3 at $t = 30s$ for the smooth dam break problem with $\beta = 1.17778$ for $\Delta x = 10/2^{10}$ (—), $\Delta x = 10/2^9$ (—), $\Delta x = 10/2^8$ (—), $\Delta x = 10/2^7$ (—), $\Delta x = 10/2^6$ (—), $\Delta x = 10/2^5$ (—), $\Delta x = 10/2^4$ (—) with reference value a^+ (—).

discontinuity will only be felt locally around the contact discontinuity and not significantly change the solution away from it. H_1 demonstrates the appropriate order of accuracy in the Hamiltonian demonstrating that we are indeed approaching a solution to this problem as Δx is increased.

The fourth scenario will be referred to as the bump scenario due to the oscillations no longer decaying down towards a point but rather growing around the contact discontinuity forming a bump as can be seen in Figure 10 for $\beta = 0.294$. This behaviour has hitherto not been published and is certainly not an expected result.

This scenario is even further from graphical convergence in Δx around the contact discontinuity than the previous scenario as can be seen in Figure 10. L_1^* demonstrates good convergence outside this middle region as can be seen in Figure 11. H_1 also converges but only has the appropriate order of accuracy in the last few Δx points. This suggests that to properly resolve this scenario requires smaller grids or higher-order

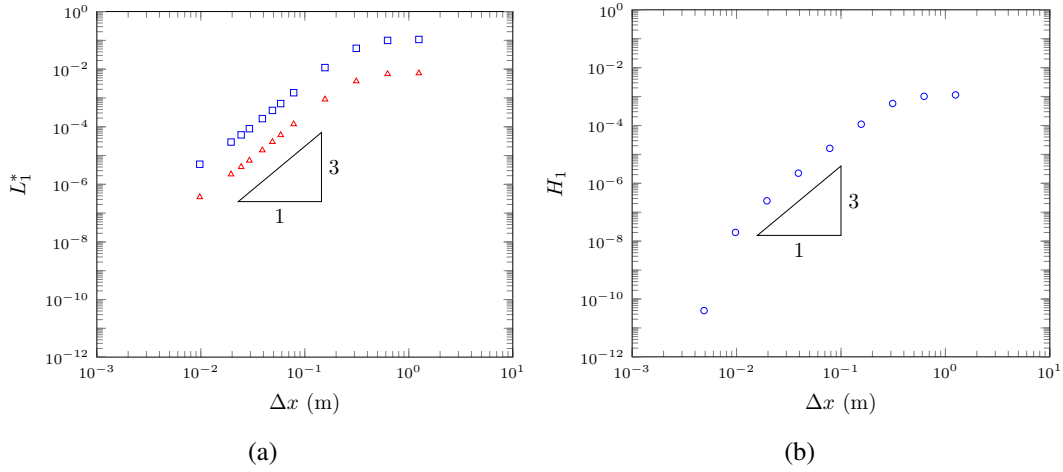


FIG. 9: L_1^* for h (\triangle) and u (\square) and H_1 (\circ) for \mathcal{V}_3 's solution for the smooth dambreak problem with $\beta = 1.17778$.

schemes. Because, convergence is not assured by these numerical results there is the possibility that the wave amplitudes around the contact discontinuity could explode. This however has not been observed, with numerical results where $\beta = 0.00294$ and $\Delta x = 10.0/2^{10}m = 0.009765625m$ at which point the initial conditions are basically a discontinuous dam break showing an increase but not an explosion in amplitude.

Since this result is unexpected and not as supported as the contact discontinuity scenario in the literature (El et al. 2006; Gurevich and Meshcherkin 1984). The first check should be different numerical methods such as \mathcal{G} and \mathcal{E} to test if some numerical effect from the reformulation of the Serre equations or the elliptic solver are the cause. For comparison all methods discussed in this paper are applied to the same initial conditions and grid resolutions as above are plotted in Figure 12. The first observation is that \mathcal{V}_1 has not recovered this behaviour. This is because as noted by Zoppou et al. (2017), \mathcal{V}_1 is very diffusive, dampening these oscillations. To resolve such behaviour for \mathcal{V}_1 would require very small Δx and as such we have not seen this behaviour yet. The diffusivity of the first-order scheme is the reason why Le Métayer et al. (2010) could not replicate the results of El et al. (2006) with reasonable Δx . Secondly, all high order methods recover this bump behaviour and disagree only in the region around the contact discontinuity. The main difference in the oscillations is their phase and amplitude with the dispersive FD methods resulting in larger waves than the diffusive FDVM.

Dispersive methods decrease oscillation amplitude and number as Δx is decreased as can be seen in Figure 14. Since \mathcal{V}_3 is diffusive as in Figure 10 the true analytic solution should then exist between \mathcal{V}_3 and \mathcal{G} , which is a bounded bump around the contact discontinuity. Finally it can be seen that \mathcal{V}_2 and \mathcal{V}_3 are similar. This is because as noted by Zoppou et al. (2017) \mathcal{V}_3 is not a substantially better method than \mathcal{V}_2 and so their results are going to be quite similar. \mathcal{G} well approximates the Serre equations, although the FDVM are still preferred by the authors due to robustness and conservation

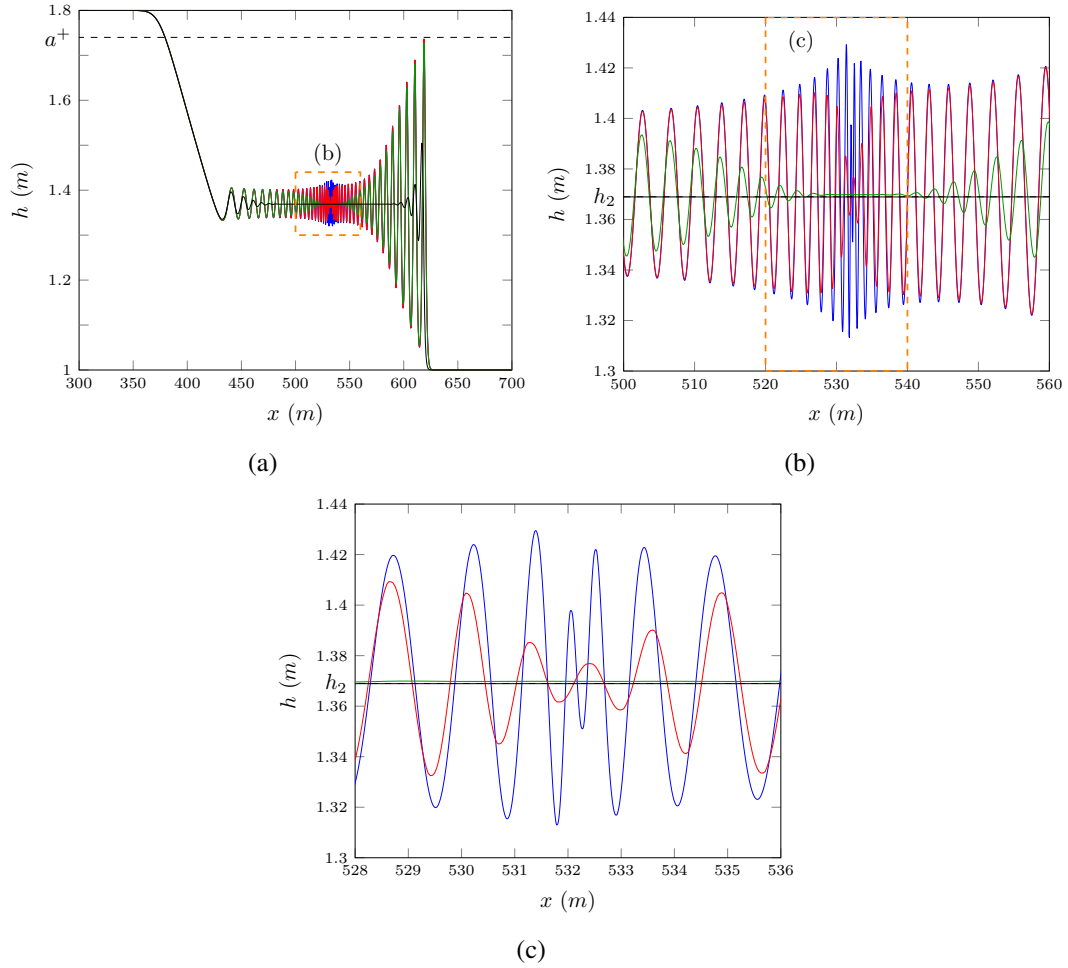


FIG. 10: Numerical results of \mathcal{V}_3 at $t = 30s$ for the smooth dam break problem with $\beta = 0.294$ for $\Delta x = 10/2^{10}$ (—), $\Delta x = 10/2^9$ (—), $\Delta x = 10/2^8$ (—), $\Delta x = 10/2^7$ (—), $\Delta x = 10/2^6$ (—), $\Delta x = 10/2^5$ (—), $\Delta x = 10/2^4$ (—) with reference value a^+ (—).

of quantities as can be seen in Figure ?? . Figure 13 demonstrates that the \mathcal{V}_i schemes result in $\mathcal{H}(30s) < \mathcal{H}(0s)$ so energy is only lost where as \mathcal{G} and \mathcal{E} can gain energy and are therefore undesirable.

There is still the possibility that these solutions are caused by some numerical phenomena such as these methods not properly handling contact discontinuities, more research into this topic should be undertaken. However, the agreement of all the discussed methods of sufficiently high order indicates that these results are representative of actual solutions of the smoothed dam break problem with low β for the Serre equations. Lastly we replicated this scenario with \mathcal{E} using a similar order of magnitude for Δx as El et al. (2006). The absence of a bump scenario in their findings is due to a smoothing of the initial conditions which is absent from the paper but was confirmed later by El and Hoefer (2016). This concludes the explanation of how our results fit in with the current literature and now the following section of this paper will be concerned

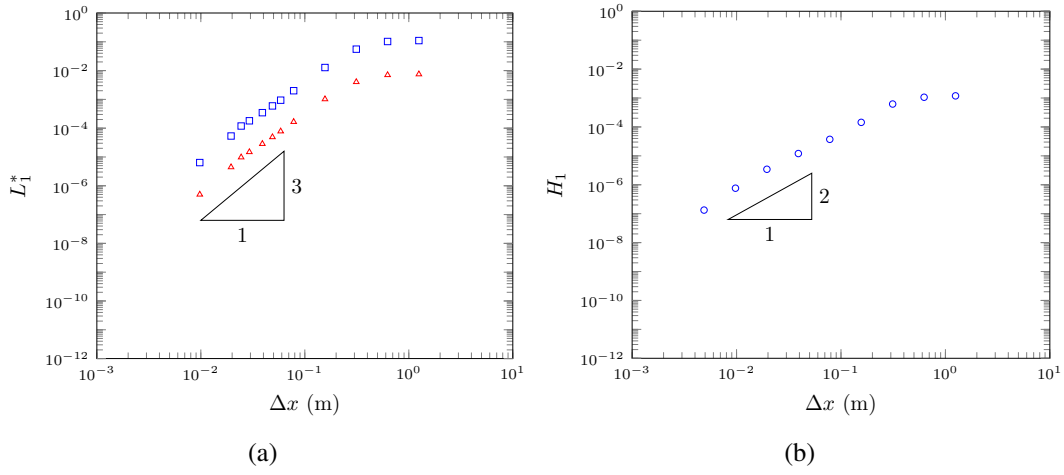


FIG. 11: L_1^* for h (\triangle) and u (\square) and H_1 (\circ) for \mathcal{V}_3 's solution for the smooth dam break problem with $\beta = 0.294$.

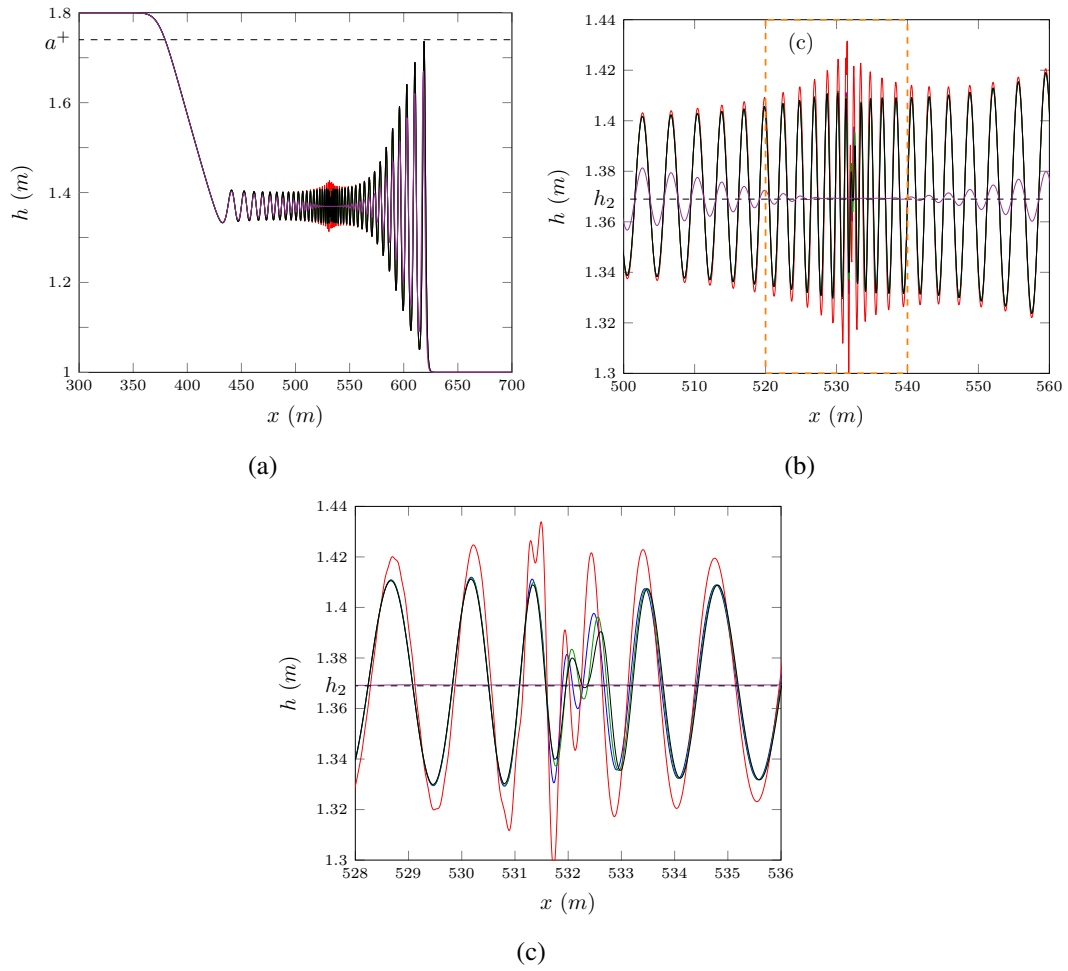


FIG. 12: Numerical results for the smooth dam break problem with $\beta = 0.294$ and $\Delta x = 10/2^{10}$ for \mathcal{G} ($-$), \mathcal{E} ($-$), \mathcal{V}_3 ($-$), \mathcal{V}_2 ($-$) and \mathcal{V}_1 ($-$) with reference value a^+ ($-$).

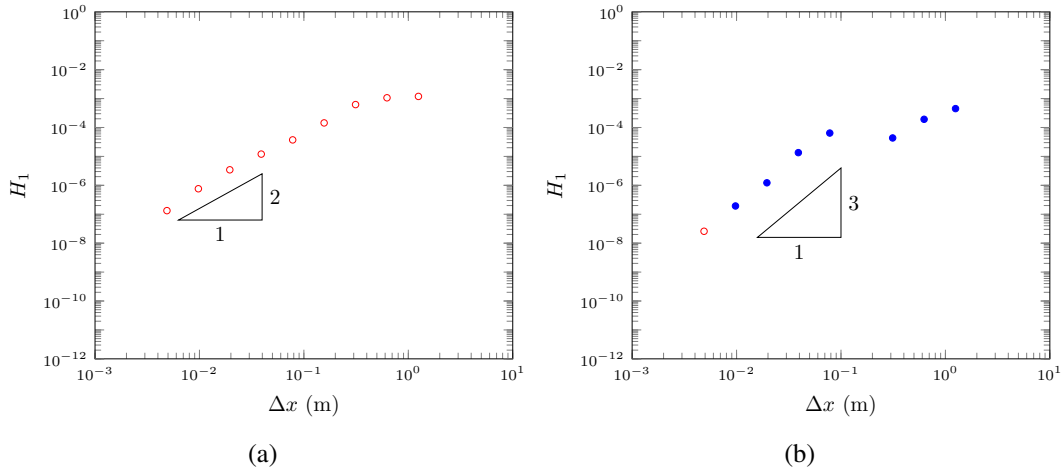


FIG. 13: H_1 for \mathcal{V}_3 (a) and \mathcal{G} 's (b) solution for the smooth dambreak problem at $t = 30s$ with $\beta = 0.294$ demonstrating when $\mathcal{H}(0s) \geq \mathcal{H}(30s)$ (\circ) and $\mathcal{H}(0s) < \mathcal{H}(30s)$ (\bullet).

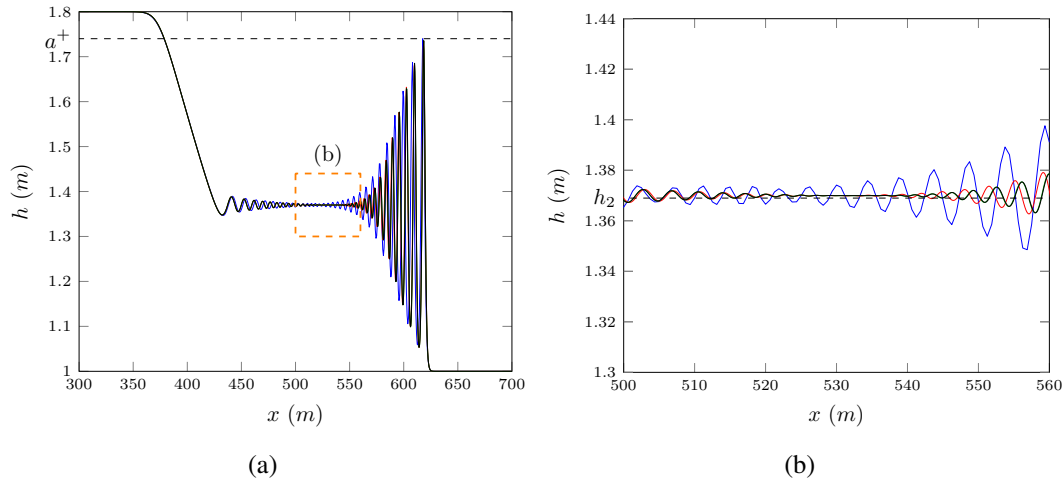


FIG. 14: Numerical results of \mathcal{G} at $t = 30s$ for the smooth dam break problem with $\beta = 5.8888$ for $\Delta x = 10/2^4$ (—), $\Delta x = 10/2^5$ (—), $\Delta x = 10/2^6$ (—), $\Delta x = 10/2^7$ (—), $\Delta x = 10/2^8$ (—), $\Delta x = 10/2^9$ (—), $\Delta x = 10/2^{10}$ (—) with reference value a^+ (—).

376 with some further numerical investigation into these results.

377 Long time

378 The first test of these results will be of its evolution through time, thus an experi-
 379 ment was run with the same parameters on a larger domain with $x \in [-900m, 1800m]$
 380 for $t \in [0, 300s]$. The results for $\beta = 0.294$ and $\Delta x = 10/2^9$ at $t = 300s$ are presented
 381 in Figure 15. For this problem these parameters result in the bump scenario as can be
 382 seen in Figure 10, however after sufficient time we can see that this bump has decayed
 383 back into a flat scenario although there are still small oscillations present in the middle
 384 region.

385 We also observe that the values S^+ and a^+ have not been perfectly replicated with

the numerical solution giving larger values than the analytic ones derived by El et al. (2006) although these results are close. We also note that as above the bore heights for the Serre and SWWE appear to be slightly different.

To observe the evolution of the water profile the numerical solution has been shifted by $u_2 \times t$ in Figure 16 to give a dam break that is essentially motionless with respect to the contact discontinuity. It can be seen that at $t = 30s$ the solution is in the bump scenario but as time progresses the centre region has decayed into the contact discontinuity scenario by $t = 100s$ and then into the flat scenario observed at $t = 200s$ and $t = 300s$. This could be a property of the solution Serre equations after sufficient time or due to the accumulation of numerical diffusion with Figure 17 demonstrating that over this timespan we are not close to convergence of the numerical results.

SWWE comparison

Since the SWWE have been used as a guide for the mean behaviour of the solution of the Serre equations in the literature (Le Métayer et al. 2010; Mitsotakis et al. 2014) we would like to investigate how useful they are. We begin by studying the speed of the contact discontinuity which should travel at the mean bore velocity (Gurevich and Meshcherkin 1984). Since as stated before there are analytic solutions for these values for the SWWE, the numerical results can be compared to this. To investigate this h_1 was varied to allow for different aspect ratios and thus different bore speeds. The results are plotted in Figure 18 from which it is quite clear that this discontinuity does in fact travel at the bore speed for a range of aspect ratios.

To further demonstrate the SWWE solution as a useful guide for mean behaviour we plot $h - h_2$ and $u - u_2$ for the smoothed dam break problem with $\beta = 0.2944$ and $\Delta x = \frac{10}{29}$ in Figure 19 for $t = 30s$ and Figure 19 for $t = 300s$. From this we can see that over short time spans both h_2 and u_2 are good approximations to the mean behaviour of the fluid with both plots oscillating around 0. However after sufficient time we see that the mean velocity and height of the fluid has diverged slightly from the SWW equation values h_2 and u_2 . With h_2 being an underestimate and u_2 being an overestimate. From Figure 15 it can also be seen that S_2 underestimates the speed of the bore front.

From Figure 19(b) and Figure 19(d) it can also be seen that to the left of the contact discontinuity u and h are antiphase. While Figure 19(c) and Figure 19(d) demonstrate that to the right of the contact discontinuity u and h are in phase. Thus the contact discontinuity marks the transition between these two states, for comparison in both 19(d) and 20(d) I have marked the point $x_2 = tu_2$ which is the point the contact discontinuity would be at if it travelled at u_2 . From 20(d) it is clear that at x_2 h and u are in phase and so x_2 is a slight overestimate of the location of the contact discontinuity as u_2 is for the speed of the contact discontinuity and u .

Because h and u are antiphase to the left of the contact discontinuity they appear to travel leftwards relative to the contact discontinuity while those on the right are in phase and therefore appear to be travelling rightwards relative to the contact discontinuity. Thus these oscillations appear to be forming at the contact discontinuity and

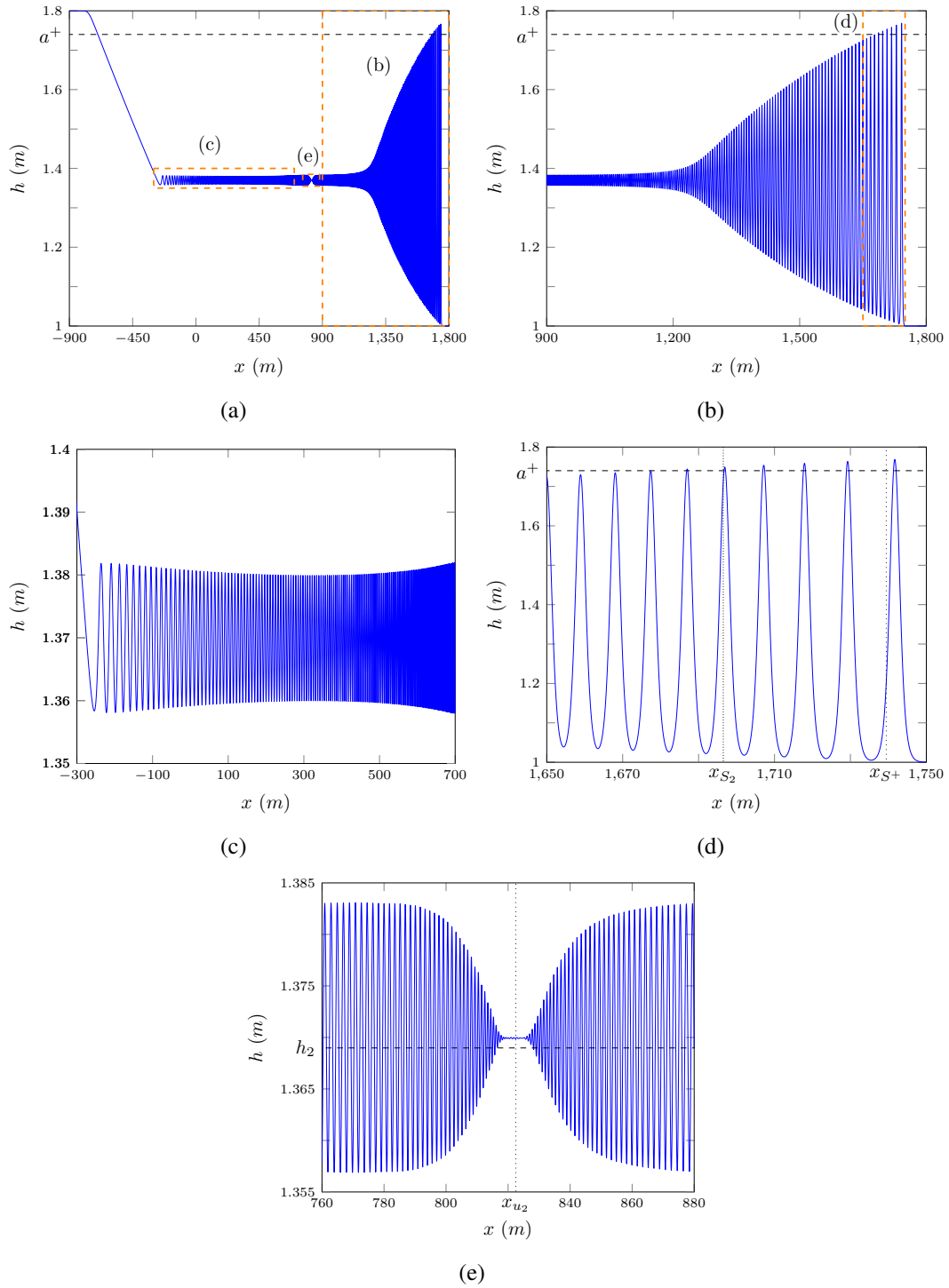


FIG. 15: Smooth dam break problem at $t = 300s$ for \mathcal{V}_3 with $\beta = 0.294$ for $\Delta x = 10/2^9$ (—) with reference values a^+ (—) ((a), (b), (d)), S^+ (\cdots) (d), S_2 ($\cdots\cdots$) (d), h_2 (—) (e) and x_2 (\cdots) (e).

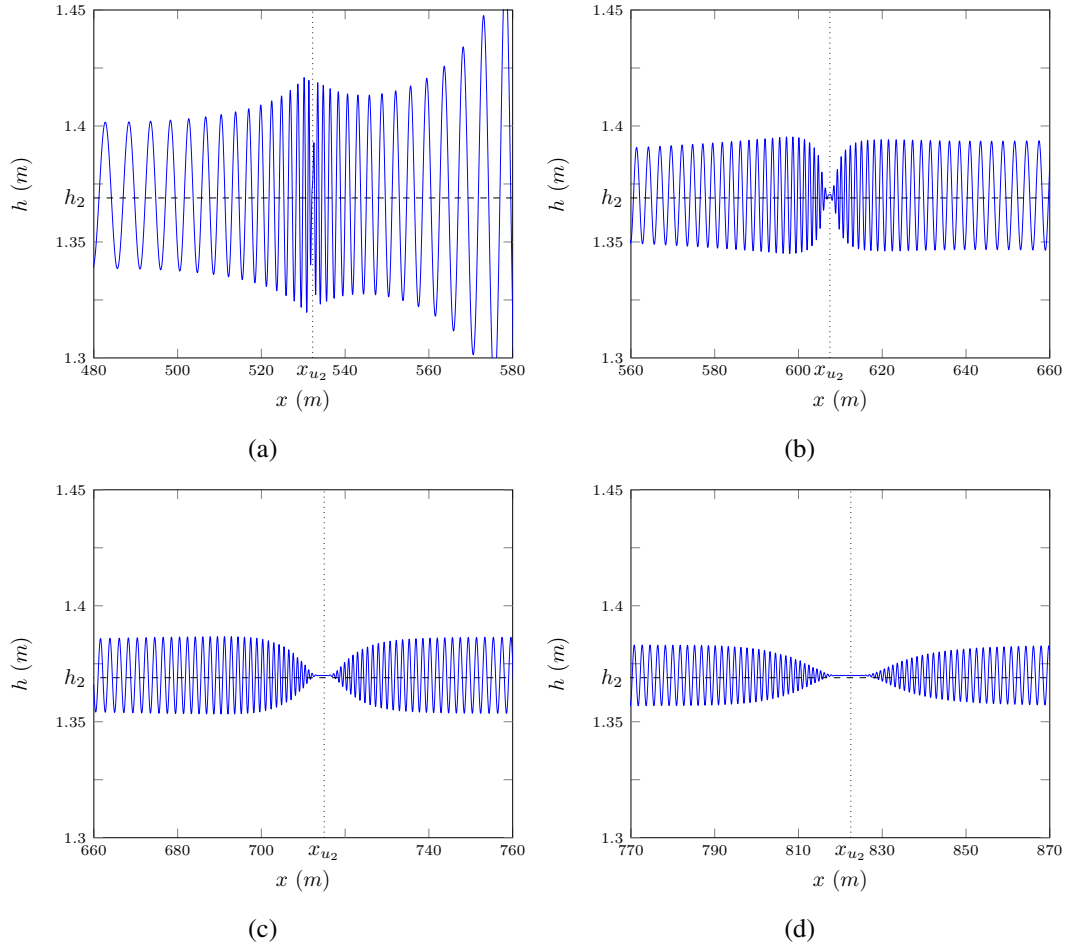


FIG. 16: Numerical solution of the smoothed dam break with \mathcal{V}_3 , $\beta = 0.294$ and $\Delta x = 10/2^9$ at $t = 30s$ (a), $100s$ (b), $200s$ (c), $300s$ (d).

then travelling away from it. The phase velocity of the linearised Serre equations is

$$v_p = u \pm \sqrt{gh} \sqrt{\frac{3}{h^2 k^2 + 3}}$$

where k is the wavenumber. The phase velocity has the following behaviour, as $k \rightarrow \infty$ then $v_p \rightarrow u$ and as $k \rightarrow 0$ then $v_p \rightarrow u \pm \sqrt{gh}$. Since we observe u and h as being antiphase to the left of the contact discontinuity this means we are in the negative branch of the phase velocity $u - \sqrt{gh} \sqrt{\frac{3}{h^2 k^2 + 3}}$ while the in phase right corresponds to the positive branch $u + \sqrt{gh} \sqrt{\frac{3}{h^2 k^2 + 3}}$. Thus the contact discontinuity corresponds to very high wavenumber oscillations, which explains why it is very sensitive to both smoothing of the initial conditions and numerical diffusion.

Whitham modulation comparison

The expressions for the lead soliton amplitude a^+ and speed S^+ obtained by El et al. (2006) are asymptotic results and so we are interested in how our numerical re-

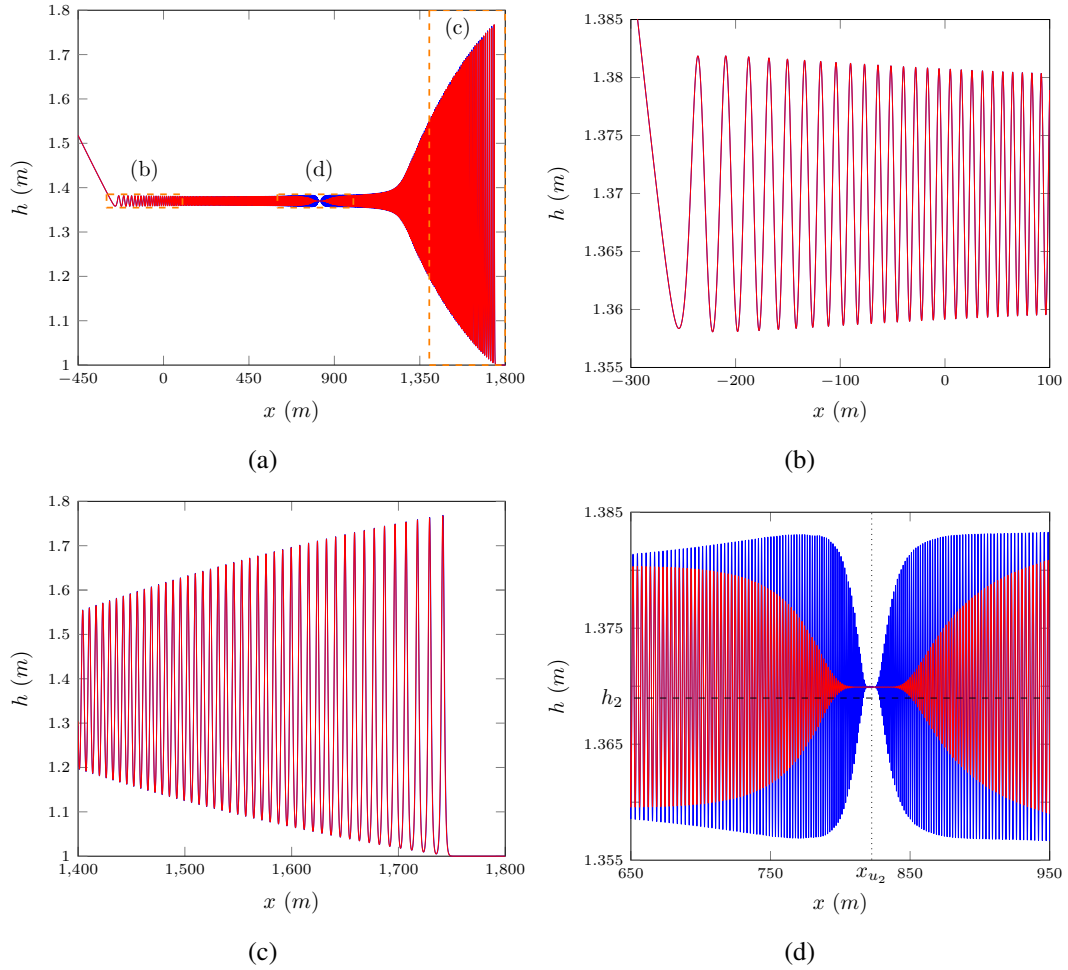
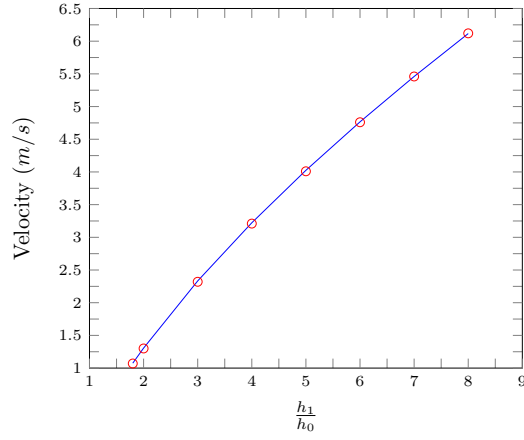


FIG. 17: Smooth dam break problem at $t = 300s$ for \mathcal{V}_3 with $\beta = 0.294$ for $\Delta x = 10/2^9$ (—) and $\Delta x = 10/2^8$ (---) with reference values h_2 (—) (d) and x_2 (···) (d).

sults behave over time. Thus for the dam break problem in the long time subsection the lead soliton amplitude was captured over time and plotted in Figure 21. From it we can see that we do appear to approach some value but that value is higher than the analytic value a^+ . We find that using larger β and larger Δx allows our numerical solution to better approach a^+ and so by better approximating the true solution we actually converge away from a^+ not towards it in this timescale for this aspect ratio. This is not inconsistent with the results of (El et al. 2006) as their scale comparing a^+ to numerical solutions is too large to see such a small difference. From Figure 15 it can be seen that while S^+ does not precisely predict the bore speed it is closer than the analytic result of the SWWE S_2 .

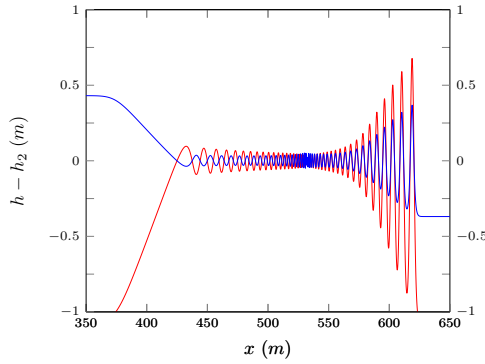
Energy Breakdown

The Hamiltonian (3) has 3 terms representing in order, horizontal kinetic energy hu^2 , gravitational potential energy gh^2 and lastly vertical kinetic energy $\frac{h^3}{3} \frac{\partial u}{\partial x}$. It might be expected that the these rapid oscillations of the undular bore such as in Figure 15

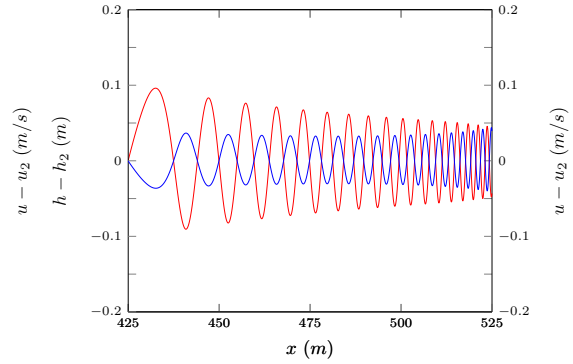


(a)

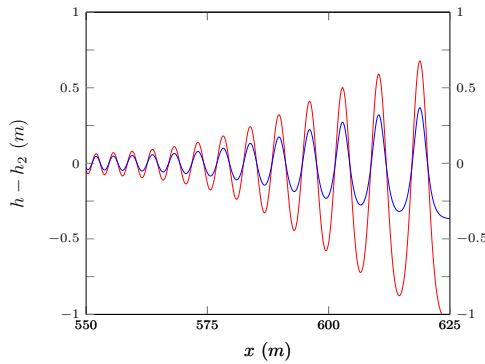
FIG. 18: u_2 (—) and speed of the contact discontinuity (\circ) for \mathcal{V}_3 solution of the various smooth dam break problems with $\beta = 0.2944$ and $\Delta x = 10/2^9$ at $t = 100s$.



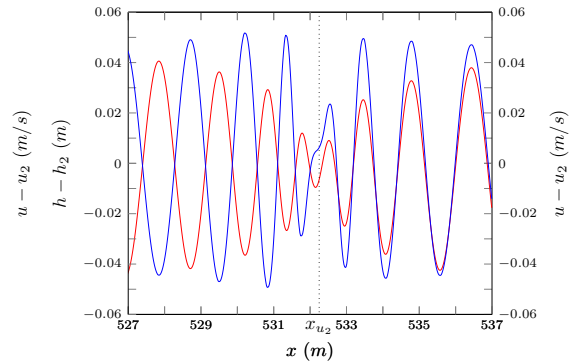
(a)



(b)



(c)



(d)

FIG. 19: $h - h_2$ (—) and $u - u_2$ (—) for \mathcal{V}_3 solution of the smooth dam break with $\beta = 0.2944$ and $\Delta x = 10/2^9$ at $t = 30s$.

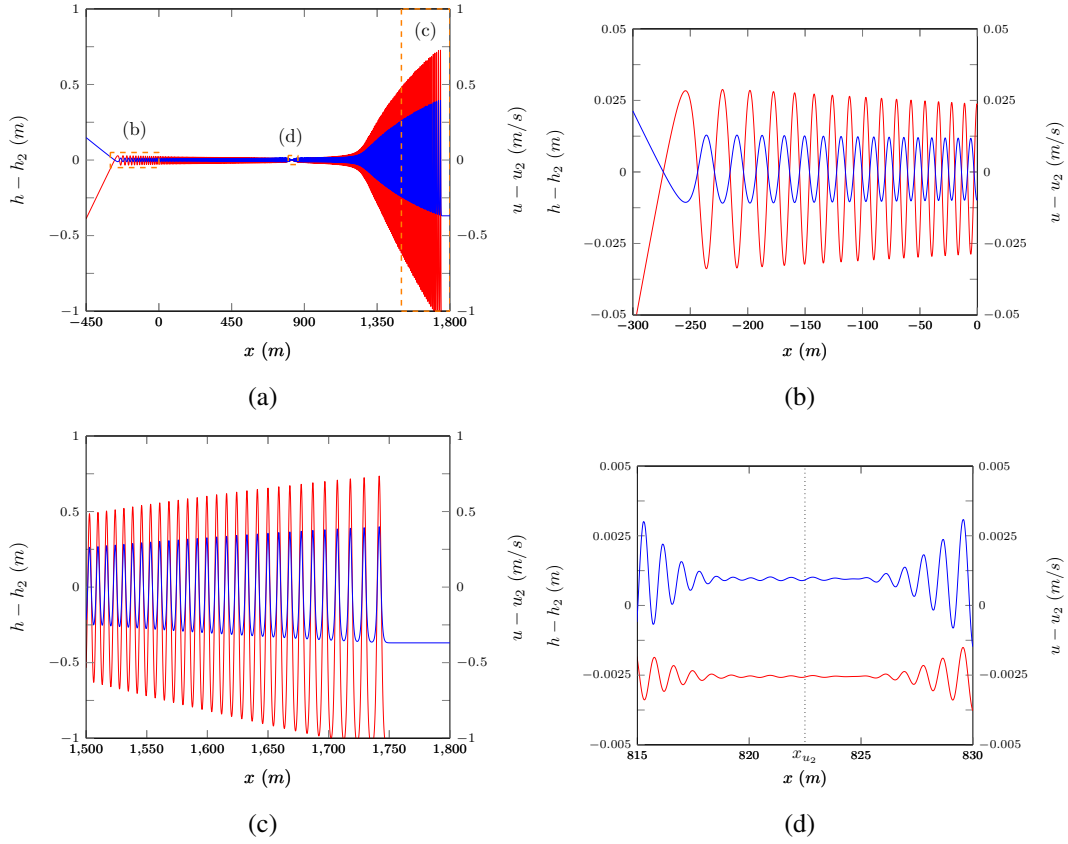


FIG. 20: $h - h_2$ (—) and $u - u_2$ (—) for \mathcal{V}_3 solution of the smooth dam break with $\beta = 0.2944$ and $\Delta x = 10/2^9$ at $t = 300s$.

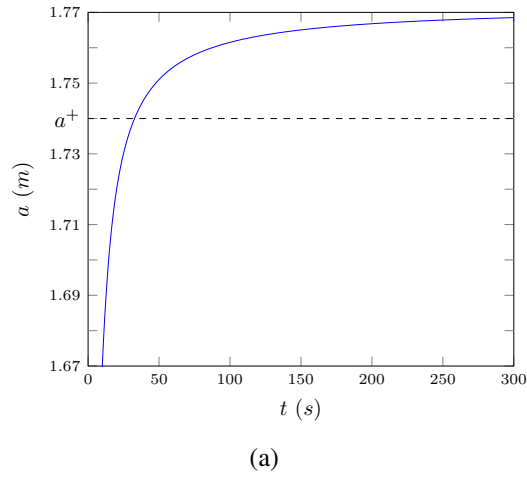


FIG. 21: Lead soliton height plotted over time for the smooth dam break problem at $t = 300s$ for \mathcal{V}_3 with $\beta = 0.294$ for $\Delta x = 10/2^9$ (—) with reference value a^+ (— —).

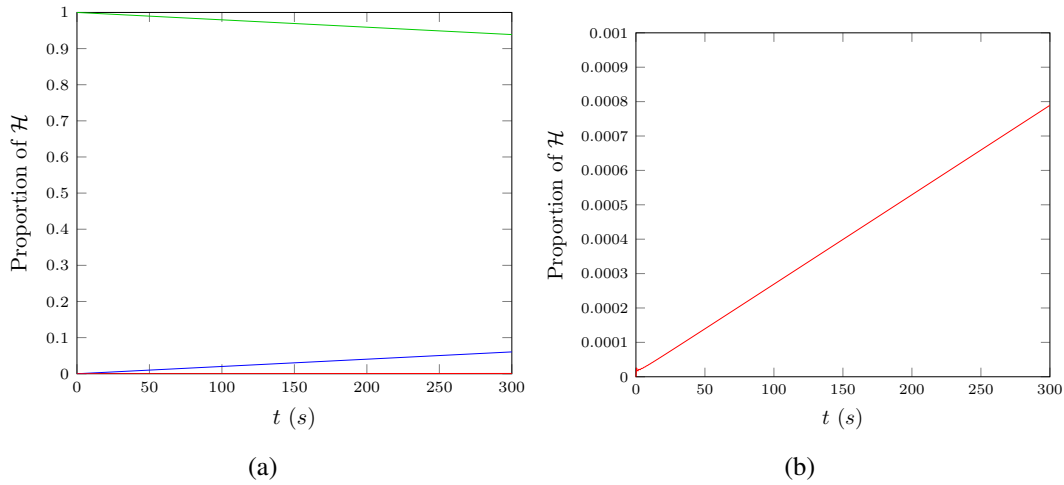


FIG. 22: Proportion of \mathcal{H} made up by horizontal kinetic energy (—) , vertical kinetic energy (—) and gravitational potential energy (—) for \mathcal{V}_3 solution of the smooth dam break with $\beta = 0.2944$ and $\Delta x = 10/2^9$ over time.

would result in significant vertical energies. However, Figure 22 demonstrates that this is not the case, as the total vertical kinetic energy in the system is insignificant relative to the other energies. This plot also demonstrates that even with dispersive terms and large oscillations the drivers of change in the dam break problem are the transfer of gravitational potential energy into horizontal kinetic energy which occurs very slowly.

CONCLUSIONS

Utilizing two finite difference methods of second order and three finite difference-volume methods of various orders an investigation into the smooth dambreak problem with various steepnesses was performed. Four different behaviours were uncovered with the general trend being that an increase in steepness increases the size and number of oscillations in the solution. This study explains all current differences in the literature involving the solution of the Serre equations applied to the smoothed dam break problem and also uncovers a new result. We find that while the analytic solution of the dam break problem is a good guide to the mean behaviour of the Serre equations the speed and height of the bores do not match up precisely. While the Whitham modulation results for the Serre equations give better predictions than the SWW analytic solution it was found that they while close do not line up with our numerical results precisely. It was also demonstrated that the contact discontinuity corresponds to high wave numbers and that vertical kinetic energy is negligible for the dam break problem.

REFERENCES

- A. Harten, A. (1983). “High resolution schemes for hyperbolic conservation laws.” *Journal of Computational Physics*, 49(3), 357–393.
- Antunes do Carmo, A., Seabra-Santos, F. J., and Almeida, A. B. (1993). “Numerical solution of the generalized Serre equations with the MacCormack finite-difference scheme.” *International Journal for Numerical Methods in Fluids*, 16(8), 725–738.

- 478 Bonneton, P., Chazel, F., Lannes, D., Marche, F., and Tissier, M. (2011). "A splitting
479 approach for the fully nonlinear and weakly dispersive Green-Naghdi model."
480 *Journal of Computational Physics*, 230(4), 1479–1498.
- 481 Bradford, S. F. and Sanders, B. F. (2002). "Finite volume schemes for the boussinesq
482 equations." *Ocean Wave Measurement and Analysis (2001)*, 953–962.
- 483 Carter, J. D. and Cienfuegos, R. (2011). "Solitary and cnoidal wave solutions of the
484 Serre equations and their stability." *European Journal of Mechanics B/Fluids*, 30(3),
485 259–268.
- 486 El, G., Grimshaw, R. H. J., and Smyth, N. F. (2006). "Unsteady undular bores in fully
487 nonlinear shallow-water theory." *Physics of Fluids*, 18(027104).
- 488 El, G. and Hoefer, M. (2016). "Dispersive shock waves and modulation theory." *Physica D: Nonlinear Phenomena*, 333, 11–65.
- 489 Filippini, A. G., Kazolea, M., and Ricchiuto, M. (2016). "A flexible genuinely non-
490 linear approach for nonlinear wave propagation, breaking and run-up." *Journal of*
491 *Computational Physics*, 310, 381–417.
- 493 Glimsdal, S., Pedersen, G. K., Harbitz, C. B., and Løvholt, F. (2013). "Dispersion
494 of tsunamis: does it really matter?." *Natural Hazards and Earth System Sciences*,
495 13(6), 1507–1526.
- 496 Green, A. E. and Naghdi, P. M. (1976). "A derivation of equations for wave propagation
497 in water of variable depth." *Journal of Fluid Mechanics*, 78(2), 237–246.
- 498 Gurevich, A. and Meshcherkin, A. (1984). "Expanding self-similar discontinuities and
499 shock waves in dispersive hydrodynamics." *Zhurnal Eksperimental'noi i Teoretich-*
500 *eskoi Fiziki*, 87, 1277–1292.
- 501 Lannes, D. and Bonneton, P. (2009)." *Physics of Fluids*, 21(1), 16601–16610.
- 502 Le Métayer, O., Gavriluk, S., and Hank, S. (2010). "A numerical scheme for the
503 GreenNaghdi model." *Journal of Computational Physics*, 229(6), 2034–2045.
- 504 Li, M., Guyenne, P., Li, F., and Xu, L. (2014). "High order well-balanced CDG-FE
505 methods for shallow water waves by a Green-Naghdi model." *Journal of Computa-*
506 *tional Physics*, 257, 169–192.
- 507 Li, Y. A. (2002). "Hamiltonian Structure and Linear Stability of Solitary Waves of the
508 Green-Naghdi Equations." *Journal of Nonlinear Mathematical Physics*, 9, 99–105.
- 509 Mitsotakis, D., Dutykh, D., and Carter, J. (2016). "On the nonlinear dynamics of the
510 traveling-wave solutions of the serre system." *Wave Motion*.
- 511 Mitsotakis, D., Ilan, B., and Dutykh, D. (2014). "On the Galerkin/Finite-Element
512 Method for the Serre Equations." *Journal of Scientific Computing*, 61(1), 166–195.
- 513 Nwogu, O. (1993). "Alternative form of Boussinesq equations for nearshore wave
514 propagation." *Journal of Waterway, Port, Coastal, and Ocean Engineering, American*
515 *Society of Civil Engineers*, 119(6), 618–638.
- 516 Peregrine, D. H. (1966). "Calculations of the development of an undular bore." *Journal*
517 *of Fluid Mechanics*, 25(2), 321–330.
- 518 Seabra-Santos, F. J., Renouard, D. P., and Temperville, A. M. (1981). "Numerical and
519 experimental study of the transformation of a solitary wave over a shelf or isolated
520 obstacle." *Journal of Fluid Mechanics*, 176, 117–134.
- 521 Serre, F. (1953). "Contribution à l'étude des écoulements permanents et variables dans

522 les canaux.” *La Houille Blanche*, 6, 830–872.
 523 Su, C. H. and Gardner, C. S. (1969). “Korteweg-de Vries equation and generalisations.
 524 III. Derivation of the Korteweg-de Vries equation and Burgers equation.” *Journal of*
 525 *Mathematical Physics*, 10(3), 536–539.
 526 Wu, C., Huang, G., and Zheng, Y. (1999). “Theoretical solution of dam-break shock
 527 wave.” *Journal of Hydraulic Engineering*, 125(11), 1210–1215.
 528 Zoppou, C. (2014). “Numerical solution of the One-dimensional and Cylindrical Serre
 529 Equations for Rapidly Varying Free Surface Flows.” Ph.D. thesis, Australian Na-
 530 tional University, Mathematical Sciences Institute, College of Physical and Mathe-
 531 matical Sciences, Australian National University, Canberra, ACT 2600, Australia.
 532 Zoppou, C., Pitt, J., and Roberts, S. (2017). “Numerical solution of the fully non-linear
 533 weakly dispersive serre equations for steep gradient flows.” *Applied Mathematical*
 534 *Modelling*, 00(00), 00–00.
 535 Zoppou, C. and Roberts, S. (2003). “Explicit schemes for dam-break simulations.”
 536 *Journal of Hydraulic Engineering, American Society of Civil Engineers*, 129(1),
 537 11–34.